Hindawi
Journal of Nanotechnology
Volume 2021, Article ID 9267962, 6 pages
https://doi.org/10.1155/2021/9267962

*Research Article*

# Multipeak Emissions and Electrical Properties of ZnO/Si Heterojunctions Based on ZnO Nanoflakes by Spin Coating Technique

**Ya Jun Ma, Peng Fei Ji, Yong Li, and Yue Li Song**

*Key Laboratory of Nano Optoelectronic Materials and Insulation Materials, Pingdingshan University, Pingdingshan 467000, China*

Correspondence should be addressed to Yue Li Song; songyl@pdsu.edu.cn

Received 1 July 2021; Revised 15 September 2021; Accepted 21 September 2021; Published 28 September 2021

Academic Editor: Marco Rossi



ZnO/Si heterojunctions have been fabricated by spinning ZnO nanoflakes on the p-type single crystal silicon by using the spin coating technique. Photoluminescence spectra of as-grown and annealed ZnO/Si heterojunctions have been recorded under the excitation of 336 nm. Multipeaks between ~360 nm and ~430 nm from annealed ZnO/Si heterojunctions have been analyzed, the origins of which have been ascribed to the effects of one or multiple LO phonons. The rectifying effects can be observed from the prototypical devices based on ZnO/Si heterojunctions. Although the parameters obtained by analyzing the current density-voltage characteristics are away from those from the ideal device, it is believed that ZnO/Si heterojunctions in the present work will be a potential candidate in the optoelectronic field through modulating and optimizing the fabrication conditions.

## 1. Introduction

As an important functional oxide semiconductor, nanostructured ZnO has offered an interesting prospect in the fields of optoelectronic devices by manipulating the morphology, doping, and structural composition [1–6]. In the perovskite solar cells, ZnO has been used as an alternative to $TiO_2$ for its high efficiency [7]. Based on the p-type silicon, ZnO has been used as an n-type material to fabricate the ZnO/Si heterojunctions. Solar cells based on ZnO/Si heterojunctions have been researched extensively by many groups, and some exciting results have been obtained [8–10]. But the efficiency of photovoltaic devices based on ZnO/Si heterojunctions is still unsatisfactory. In order to improve the performance, for instance, Pietruszka and Knutsen have incorporated a $Zn_{1-x}Mg_xO$ layer into the ZnO-Si interface to modulate the conduction band offset, which can lead to a diminishing impact of recombination centers at the interface [9, 10]. Hussain has deposited amorphous ZnO at the interface of ZnO-Si to improve the interface passivation and decrease the oxide formation, and the open circuit voltage shows more than 20% improvement [8]. Zhong's group has doped Al in ZnO to construct an efficient electron-selective contact to enhance the performance [11]. In the study of light emitting diodes, Fang's research group has incorporated $HfO_2$ into the heterojunction interface to improve the light emission of ZnO/Si heterojunctions [12–14]. Another way to improve device performance is to fabricate high-quality ZnO to construct the high efficiency optoelectronic devices. The pulsed laser deposition and metal organic chemical vapor deposition have been applied, which are expensive and carried out in the high vacuum atmosphere [15]. The spin coating technique is a simple method, which is characterized with many benefits, for example, cost effectiveness, absence of vacuum, and ease of fabrication of large area film on simple or complex substrates [16, 17].

In the present work, ZnO/Si heterojunctions have been fabricated through the spin coating technique. Under the excitation of 336 nm, photoluminescence (PL) spectra of as-grown and annealed ZnO/Si heterojunctions have been recorded, and the origins of multipeaks have been investigated. And, the electronic parameters of prototypical device

based on annealed ZnO/Si heterojunctions have been analyzed.

## 2. Experiments

The preparation of ZnO nanoflakes is as follows. First, the analytical reagents, zinc nitrate (0.015 mol) and sodium hydroxide (0.06 mol), were mixed into 70 ml deionized water. The mixture was shifted into an autoclave which was filled with ~70% solution and fixed in the oven. The temperature in the oven rose from room temperature to 160°C for 30 min. After lasting for 2 h at 160°C, the autoclave was taken out from the oven. After natural cooling for 1.5 h, the white precipitant in the autoclave was washed three times with the deionized water, and then it was filtered and dried. And then, the white precipitant was added into the ethanol and stirred for 20 min at room temperature. The p-type single crystal silicon was placed on the spin coating platform, and then the solution was dropped on the silicon substrate. The spin coater was set at 2000 rpm for 5 min. The above-mentioned process was repeated until the required thickness was obtained. The coated silicon substrate was dried in air atmosphere for 1 h and then split into two parts. For comparison, one of them was annealed at 300°C in argon atmosphere for 2 h. In order to investigate the electrical properties of ZnO/Si heterojunctions, the Ag electrodes were fabricated on the ZnO thin films and silicon, respectively, by using the DC magnetron sputtering method, and sandwich structure of Ag/ZnO/Si/Ag was constructed.

The morphological and structural properties of the ZnO nanoflakes, as-grown and annealed ZnO/Si heterojunctions, were characterized by field emission scanning electron microscopy (FE-SEM, JSM 6700F) at an acceleration voltage of 15 kV; high-resolution transmission electron microscopy (HR-TEM, JEM-2100F) at an acceleration voltage of 200 kV; and X-ray diffraction (XRD, Panalytical X'Pert Pro) with Cu-K$\alpha$ as the X-ray source ($\lambda = 1.5046$ Å). The absorption spectrum of the annealed ZnO/Si heterojunctions was obtained using a UV-vis-IR spectrophotometer (Shimadzu, UV-3150) with an integrating sphere detector. PL spectra were measured using a double grating spectrofluorometer (HORIBA, FL3-22), with a Xe lamp as the excitation source. The current density-voltage (I-V) properties were carried out at a RST 5200 electrochemical workstation (SRS Instrument Inc., China).

## 3. Results and Discussion

XRD patterns of ZnO nanoflakes, as-grown and annealed ZnO/Si heterojunctions, are shown in Figure 1(a). The peaks located at ~31.7°, ~34.4°, ~36.2°, ~47.5°, ~56.6°, ~62.9°, and ~67.9° correspond to the diffractions of (100), (002), (101), (102), (110), (103), and (112) planes from ZnO (JCPDS: 01-089-7102), respectively. Through contrasting XRD patterns of as-grown and annealed ZnO/Si heterojunctions, the full width at half maximum (FWHM) of diffraction peaks from annealed ZnO/Si is much less than that of as-grown ZnO/Si heterojunctions. It is indicated that the size of nanostructural ZnO from ZnO/Si heterojunctions is increased after annealing treatment.

The inset of Figure 1(b) shows the morphology of annealed ZnO/Si heterojunctions. In order to study the fine structure, ZnO has been peeled off from the annealed ZnO/Si heterojunctions and been shifted to a copper net to measure. Figure 1(b) gives the TEM image of ZnO nanoflakes. The HR-TEM images of locations marked by asterisk and pentagram in Figure 1(b) are shown in Figures 1(c) and 1(d), respectively. From Figures 1(c) and 1(d), we can observe many zones with the obvious lattice fringes of which distances are measured and shown. The lattice fringes with ~0.278 nm and ~0.259 nm can be obtained, corresponding to the (100) and (002) planes, respectively. From SEM, TEM, and HR-TEM images, it is concluded that the size contribution of ZnO nanoflakes is large by using the provided prepared method in the present work. How to obtain the uniform size of ZnO nanostructure will be done in our future work.

Under the excitation of 336 nm, two emission bands from PL spectra of as-grown and annealed ZnO/Si heterojunctions can be obtained and illustrated in Figure 2(a). The UV emission band and blue-green emission band are located between ~360 nm and ~430 nm and between ~430 nm and ~600 nm, respectively. The inset of Figure 2(a) gives the absorptance spectrum and the plot of $(F(R)h\nu)^2$ vs. $h\nu$ from annealed ZnO/Si heterojunctions [18]. Through analyzing the plot of $(F(R)h\nu)^2$ vs. $h\nu$, the band gap of annealed ZnO/Si heterojunctions can be calculated to be ~3.316 eV (~374 nm) [19, 20]. So, it is believed that the UV emission is ascribed to the emission of band gap from ZnO nanoflakes. However, a significant red-shift compared to the calculated band gap can be observed, which is attributed to more surface defects [21]. Oxygen vacancies are located at ~0.9 eV above the valence band of ZnO [22–25]. Combined with the obtained band gap of ZnO nanoflakes, we think that the blue-green emission is originated from the transition from the conduction band to oxygen vacancies. For PL spectrum of as-grown ZnO/Si heterojunctions, the intensity of UV emission is much less than that of blue-green emission. After the annealing treatment has been carried out, however, the intensity of UV emission has greatly been improved. The peak positions of UV and blue-green emissions are independent of the annealed treatment. While for PL of annealed ZnO/Si heterojunctions, multiple peaks can be observed between ~360 nm and ~430 nm, which are located at ~375 nm (~3.307 eV), ~385 nm (~3.221 eV), ~395 nm (~3.139 eV), ~406 nm (~3.054 eV), and ~418 nm (~2.967 eV) from short wavelength to long wavelength, respectively. The energy differences between adjacent peaks can be estimated to be ~86 meV, ~82 meV, ~85 meV, and ~87 meV, respectively. In the works of Dingle and Reynolds [26, 27], LO phonon of ~72 meV had been discussed in the emission bands of ZnO. In the present work, the multiple LO phonons have been ascribed to the multipeaks between ~360 nm and ~430 nm [14, 28, 29].

In order to investigate the emission dynamics, [30] the decay curves of the PL spectrum from annealed ZnO/Si heterojunctions at ~393 nm and ~500 nm under the 450 nm

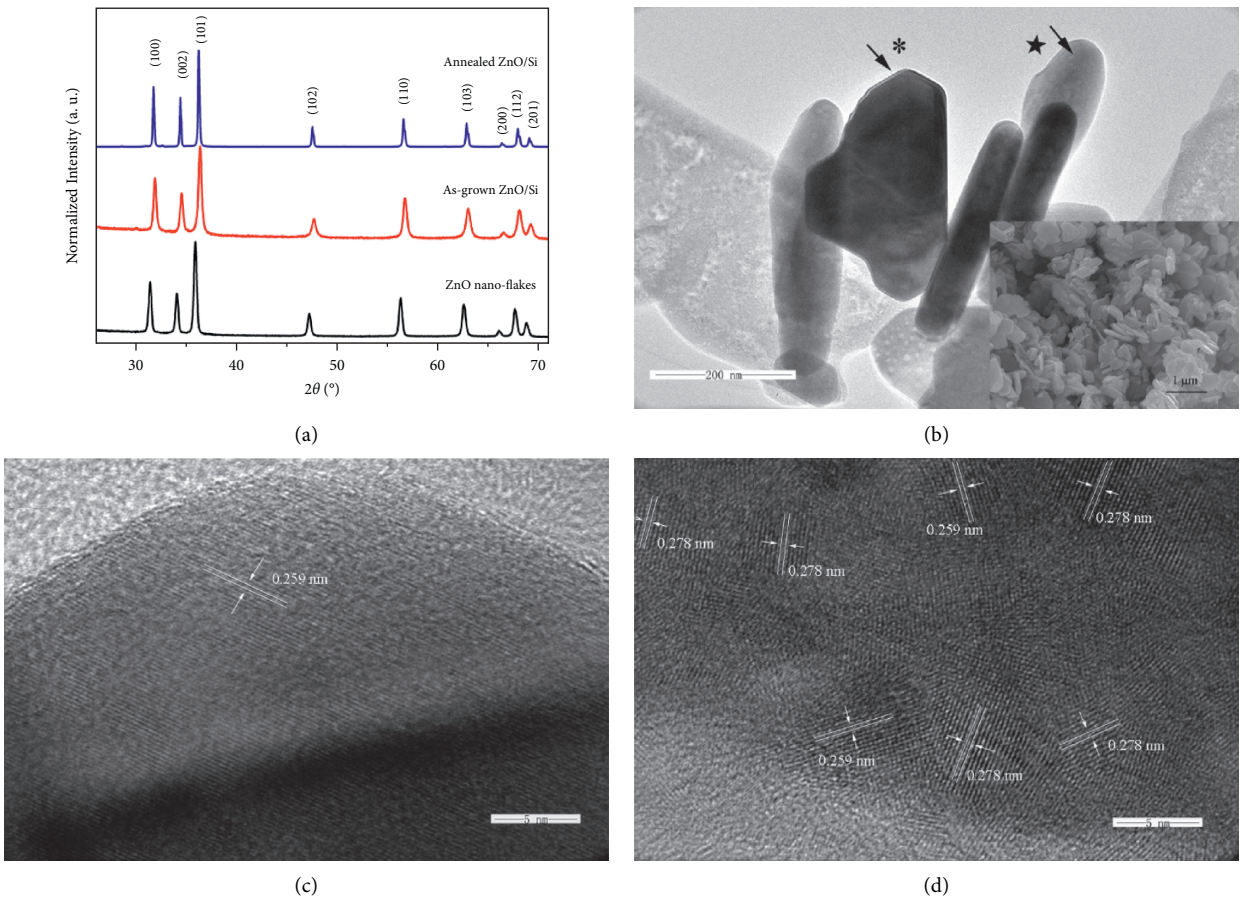


FIGURE 1: (a) XRD patterns from ZnO nanoflakes, as-grown and annealed ZnO/Si heterojunctions. (b) TEM image of ZnO peeled off from annealed ZnO/Si heterojunctions. Inset: top view of annealed ZnO/Si heterojunctions. (c, d) HR-TEM images from the locations marked by asterisk and pentagram, respectively.

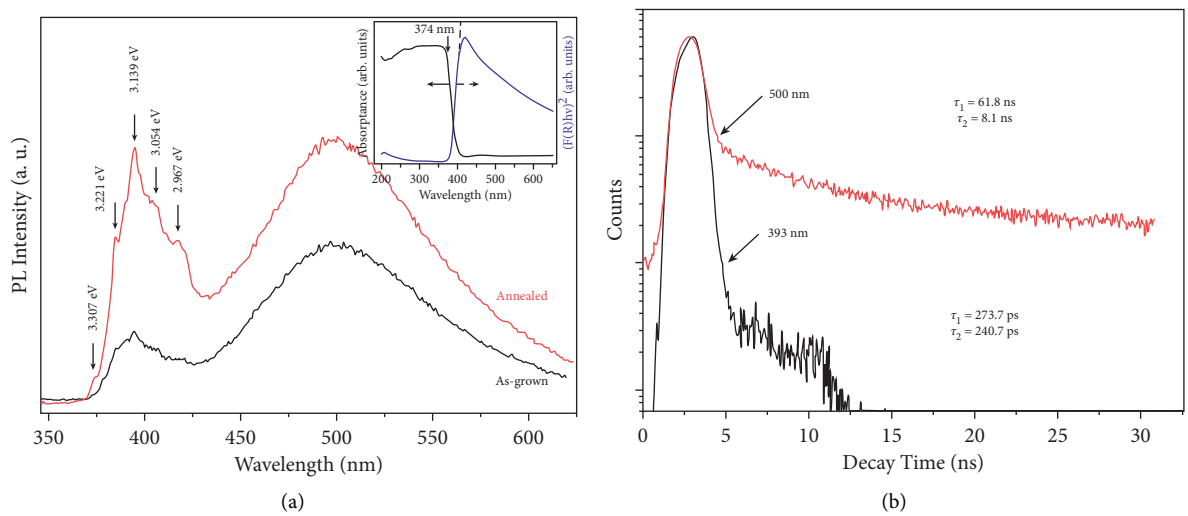


FIGURE 2: (a) PL spectra of as-grown and annealed ZnO/Si heterojunctions. Inset: the plot of $(F(R)h\nu)^2$ vs. $h\nu$ from annealed ZnO/Si heterojunctions. (b) Decay curve of PL from annealed ZnO/Si heterojunctions at ~393 nm and ~500 nm.

excitation are analyzed and shown in Figure 2(b). The data are fitted by the biexponential decay function as follows [29, 31]:

$$A(t) = A_1 \exp\left(\frac{-t}{\tau_1}\right) + A_2 \exp\left(\frac{-t}{\tau_2}\right), \quad (1)$$

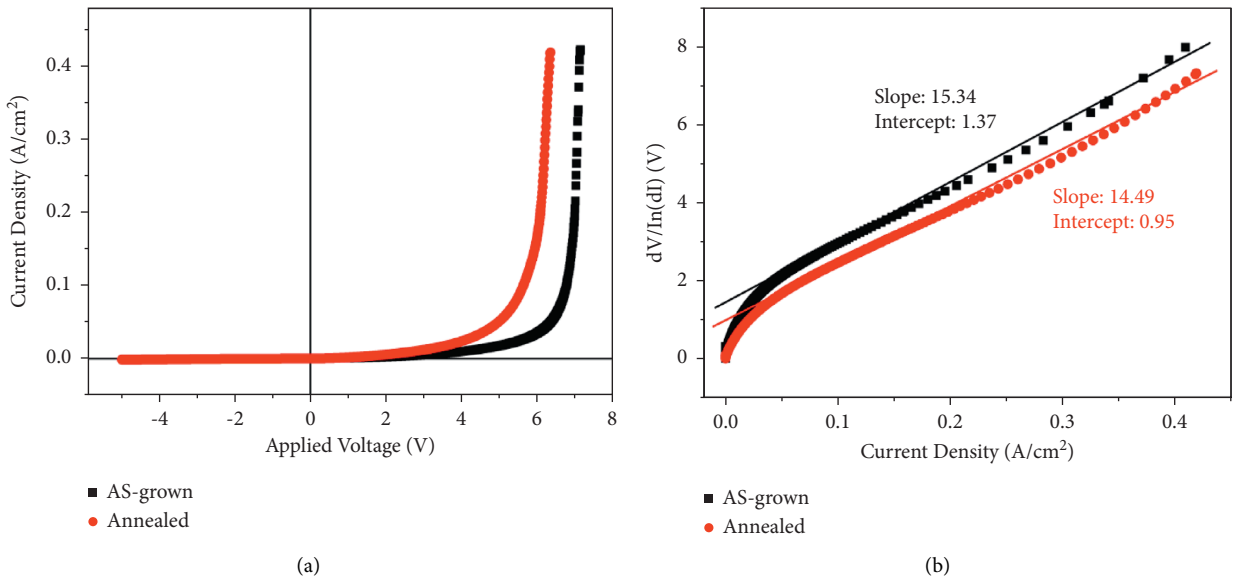


Figure 3: (a) I-V and (b) d$V$/d(ln$I$)-I properties from as-grown and annealed ZnO/Si heterojunctions.

where $A(t)$ represents the emission band intensity and $A_1$ and $A_1$ are the relative weights of two exponential decays with the time constants $\tau_1$ and $\tau_2$, respectively. Through analyzing equation (1), the estimated decay time constants $\tau_1$ and $\tau_2$ are ~273.7 ps and ~240.7 ps for the UV emission band and ~61.8 ns and ~8.05 ns for the blue-green emission band, respectively. For the UV emission band, the lifetime of ~273.7 ps is attributed to bound exciton recombination, and the lifetime of ~240.7 ps originates from free exciton recombination [29]. For the blue-green emission band, the lifetimes of ~61.8 ns and ~8.1 ns originate from the defects near the ZnO nanoflake surface [32].

I-V characteristics of as-grown and annealed Ag/ZnO/Si/Ag heterojunctions have been measured at room temperature and shown in Figure 3(a). From Figure 3(a), the obvious rectification effects are observed. For the as-grown ZnO/Si heterojunctions, the forward current density of ~0.05 mA/cm$^2$ has been obtained at the forward applied voltage of ~6.36 V. For the annealed ZnO/Si heterojunctions, however, at the forward applied voltage of ~6.36 V, the forward current density is ~0.42 mA/cm$^2$. And, it can be also observed that the onset voltage at the current density of ~1.0 mA/cm$^2$ is decreased from ~1.46 V to ~0.81 V after the annealing treatment.

In order to study the parameters of prototypical devices based on ZnO/Si in the present work, the plots of d$V$/d(ln$I$)-I by analyzing the I-V characteristics are shown in Figure 3(b), which can be expressed as follows [33]:

$$\frac{dV}{d\ln I} = IR_S + \frac{nkT}{q}, \quad (2)$$

where $I$ is the current density, $R_S$ is the series resistance, $n$ is the ideality factor, $k$ is the Boltzmann constant, $q$ is the electron charge, and $T$ is the temperature which is set to 300 K in the present work. According to equation (2), the slopes and intercepts can be obtained by using the linear fit and are shown in Figure 3(b). The series resistances can be estimated from the slops of fitted lines and be calculated to be ~15.34 Ohm/cm$^2$ and ~14.5 Ohm/cm$^2$ for as-grown and annealed ZnO/Si heterojunctions, respectively. And, the ideality factors, which can be estimated from the intercept of fitted line [34], are ~53.7 and ~37.2, respectively. It is indicated that the annealed treatment can enhance the performance of ZnO/Si heterojunctions. Although the obtained parameters, such as ideality factor, are away from the those of ideal devices [35], it is believed that the performance based on ZnO/Si heterojunctions by the spin coating technique at the present work can be improved through modulating and optimizing the preparation conditions.

## 4. Conclusion

ZnO/Si heterojunctions have been fabricated through the spin coating technique. In the UV emission band of annealed ZnO/Si heterojunctions, multipeaks have been observed. The origins of emission bands have been discussed in detail. After annealing treatment, the performance of ZnO/Si heterojunctions device has been improved. However, the obtained electrical parameters are away from those of the ideal device. It is believed that ZnO/Si heterojunctions in the present work will be a promising candidate in the optoelectronic device fields through optimizing the preparation conditions.

## Data Availability

The data used to support the finding of this study are included within the article.

## Conflicts of Interest

The authors declare that there are no conflicts of interest regarding the publication of this paper.

## Authors' Contributions

Ya Jun Ma and Pengfei Ji were responsible for acquisition, analysis, or interpretation of data for the work. Yong Li took part in drafting the work or revising it critically for important intellectual content. Yueli Song agreed to be accountable for all aspects of the work in ensuring that questions related to the accuracy or integrity of any part of the work are appropriately investigated and resolved.

## Acknowledgments

This work was supported by the Natural Science Foundation of Henan Province (Grant no. 202300410304) and the Key Research Project for Science and Technology of the Education Department of Henan Province (Grant no. 21A140021).

## References

[1] C.-L. Hsu and S.-J. Chang, "Doped ZnO 1D nanostructures: synthesis, properties, and photodetector application," *Small*, vol. 10, no. 22, pp. 4562–4585, 2014.

[2] X. Fang, Y. Bando, U. K. Gautam et al., "ZnO and ZnS nanostructures: ultraviolet-light emitters, lasers, and sensors," *Critical Reviews in Solid State and Materials Sciences*, vol. 34, no. 3-4, pp. 190–223, 2009.

[3] Z. Pan, W. Peng, F. Li, Y. Cai, and Y. He, "On the piezo-phototronic effect in Si/ZnO heterojunction photodiode: the effect of the fermi-level difference," *Advanced Functional Materials*, vol. 30, no. 51, Article ID 2005996, 2020.

[4] M. A. Fagier, "Plant-mediated biosynthesis and photo catalysis activities of zinc oxide nanoparticles: a prospect towards dyes mineralization," *Journal of Nanotechnology*, vol. 2021, Article ID 6629180, 15 pages, 2021.

[5] R. T. Ngaloy, A. M. Fontanilla, M. S. R. Soriano, C. S. Pascua, Y. Matsushita, and I. J. A. Agulo, "Highly efficient photo catalysis by zinc oxide-reduced graphene oxide (ZnO-rGO) composite synthesized via one-pot room-temperature chemical deposition method," *Journal of Nanotechnology*, vol. 2019, Article ID 1895043, 11 pages, 2019.

[6] G. Zhu, "Investigation of the mode structures of multiphoton induced ultraviolet laser in a ZnO microrod," *Journal of Nanotechnology*, vol. 2017, Article ID 3931210, 5 pages, 2017.

[7] J. Luo, Y. Wang, and Q. Zhang, "Progress in perovskite solar cells based on ZnO nanostructures," *Solar Energy*, vol. 163, pp. 289–306, 2018.

[8] B. Hussain, "Improvement in open circuit voltage of n-ZnO/p-Si solar cell by using amorphous-ZnO at the interface," *Progress in Photovoltaics: Research and Applications*, vol. 25, no. 11, pp. 919–927, 2017.

[9] K. E. Knutsen, R. Schifano, E. S. Marstein, B. G. Svensson, and A. Y. Kuznetsov, "Prediction of high efficiency ZnMgO/Si solar cells suppressing carrier recombination by conduction band engineering," *Physica Status solidi (a)*, vol. 210, pp. 585–588, 2013.

[10] R. Pietruszka, R. Schifano, T. A. Krajewski et al., "Improved efficiency of *n*-ZnO/p-Si based photovoltaic cells by band offset engineering," *Solar Energy Materials and Solar Cells*, vol. 147, pp. 164–170, 2016.

[11] S. Zhong, M. Morales-Masis, M. Mews et al., "Exploring co-sputtering of ZnO:Al and SiO2 for efficient electron-selective contacts on silicon solar cells," *Solar Energy Materials and Solar Cells*, vol. 194, pp. 67–73, 2019.

[12] Z. Chen, B. Li, X. Mo et al., "Improved light emission from *n*-ZnO/p-Si heterojunction with HfO 2 as an electron blocking layer," *Journal of Luminescence*, vol. 184, pp. 211–216, 2017.

[13] X. Mo, H. Long, H. Wang et al., "Enhanced ultraviolet electroluminescence and spectral narrowing from ZnO quantum dots/GaN heterojunction diodes by using high-k HfO2 electron blocking layer," *Applied Physics Letters*, vol. 105, no. 6, Article ID 063505, 2014.

[14] Y. Zhang, B. Lin, X. Sun, and Z. Fu, "Temperature-dependent photoluminescence of nanocrystalline ZnO thin films grown on Si (100) substrates by the sol-gel process," *Applied Physics Letters*, vol. 86, no. 13, Article ID 131910, 2005.

[15] H. Wang, Y. Zhao, C. Wu et al., "Ultraviolet electroluminescence from *n*-ZnO/NiO/p-GaN light-emitting diode fabricated by MOCVD," *Journal of Luminescence*, vol. 158, pp. 6–10, 2015.

[16] H.-K. Kim, K.-B. Chung, and J. Kal, "Comparison of ZnO buffer layers prepared by spin coating or RF magnetron sputtering for application in inverted organic solar cells," *Journal of Alloys and Compounds*, vol. 778, pp. 487–495, 2019.

[17] L. Chotirat, S. Niyomwas, W. Wongpisan, and S. Supothina, "Low-temperature synthesis of vanadium dioxide thin films by sol-gel dip coating method," *Journal of Nanotechnology*, vol. 2021, Article ID 4868152, 7 pages, 2021.

[18] A. F. Gualdrón-Reyes, A. M. Meléndez, J. Tirado, M. A. Mejia-Escobar, F. Jaramillo, and M. E. Niño-Gómez, "Hidden energy levels? Carrier transport ability of CdS/CdS1-xSex quantum dot solar cells impacted by Cd-Cd level formation," *Nanoscale*, vol. 11, no. 2, pp. 762–774, 2019.

[19] Y. Li, S. Qing Yuan, and X. Jian Li, "White light emission from CdS/Si nanoheterostructure array," *Materials Letters*, vol. 136, pp. 67–70, 2014.

[20] R. López and R. Gómez, "Band-gap energy estimation from diffuse reflectance measurements on sol-gel and commercial TiO2: a comparative study," *Journal of Sol-Gel Science and Technology*, vol. 61, no. 1, pp. 1–7, 2012.

[21] A. Nag and D. D. Sarma, "White light from Mn2+-doped CdS nanocrystals: a new approach," *Journal of Physical Chemistry C*, vol. 111, no. 37, pp. 13641–13644, 2007.

[22] S. Vempati, J. Mitra, and P. Dawson, "One-step synthesis of ZnO nanosheets: a blue-white fluorophore," *Nanoscale Research Letters*, vol. 7, no. 1, p. 470, 2012.

[23] T. K. Pathak, R. E. Kroon, L. P. Purohit, and H. C. Swart, *Spectroscopy of Lanthanide Doped Oxide Materials*, Woodhead Publishing, Sawston, UK, 2020.

[24] S. B. Zhang, S. H. Wei, and A. Zunger, "Intrinsic n-type versus p-type doping asymmetry and the defect physics of ZnO," *Physical Review B*, vol. 63, Article ID 075205, 2001.

[25] L. S. Vlasenko and G. D. Watkins, "Optical detection of electron paramagnetic resonance in room-temperature electron-irradiated ZnO," *Physical Review B*, vol. 71, no. 12, Article ID 125210, 2005.

[26] D. C. Reynolds, D. C. Look, and B. Jogai, "Fine structure on the green band in ZnO," *Journal of Applied Physics*, vol. 89, no. 11, pp. 6189–6191, 2001.

[27] R. Dingle, "Luminescent transitions associated with divalent copper impurities and the green emission from semiconducting zinc oxide," *Physical Review Letters*, vol. 23, no. 11, pp. 579–581, 1969.

[28] J. C. Johnson, K. P. Knutsen, H. Yan et al., "Ultrafast carrier dynamics in single ZnO nanowire and nanoribbon lasers," *Nano Letters*, vol. 4, no. 2, pp. 197–204, 2004.

[29] J. Dai, J. Lu, F. Wang, J. Guo, N. Gu, and C. Xu, "Optical and exciton dynamical properties of a screw-dislocation-driven ZnO : Sn microstructure," *ACS Applied Materials & Interfaces*, vol. 7, no. 23, pp. 12655–12662, 2015.

[30] B. Xu, H. Chen, T. Zhang et al., "High quality quarternary-alloyed ZnCdSSe/ZnS quantum dots with single photo-luminescence decay channel and high devise stability," *Journal of Luminescence*, vol. 240, Article ID 118463, 2021.

[31] X. Xu, Y. Zhao, E. J. Sie et al., "Dynamics of bound exciton complexes in CdS nanobelts," *ACS Nano*, vol. 5, no. 5, pp. 3660–3669, 2011.

[32] M. Jones and G. D. Scholes, "On the use of time-resolved photoluminescence as a probe of nanocrystal photoexcitation dynamics," *Journal of Materials Chemistry*, vol. 20, no. 18, pp. 3533–3538, 2010.

[33] D. E. Yıldız, Ş. Altındal, and H. Kanbur, "Gaussian distribution of inhomogeneous barrier height in Al/$SiO_2$/p-Si Schottky diodes," *Journal of Applied Physics*, vol. 103, Article ID 124502, 2008.

[34] S. K. Cheung and N. W. Cheung, "Extraction of Schottky diode parameters from forward current-voltage characteristics," *Applied Physics Letters*, vol. 49, no. 2, pp. 85–87, 1986.

[35] C. Hyun Kim, O. Yaghmazadeh, Y. Bonnassieux, and G. Horowitz, "Modelling the low-voltage regime of organic diodes: origin of the ideality factor," *Journal of Applied Physics*, vol. 110, no. 9, Article ID 093722, 2011.